Efficiency of a Cryogenic Far-Infrared Diffraction Grating Spectrometer Used as a Post-Dispersing Module

Alicia Anderson[1,2], David Naylor[2], Brad Gom[2], Ian Veenendaal[3], Adam Christiansen[1,2], Willem Jellema[4], Peter Ade[5]

[1]Blue Sky Spectroscopy Inc., Lethbridge, Canada, [2]Astronomical Instrumentation Group, University of Lethbridge, [3]SRON Netherlands Institute for Space Research, [4]Kapteyn Astronomical Institute, University of Groningen, [5]School of Physics and Astronomy, Cardiff University.

Introduction

The next generation of far-infrared astronomical space telescopes will employ a high-resolution Fourier transform spectrometer (FTS) coupled to ultra-sensitive ($\sim 10^{-19}$W / $\sqrt{\text{Hz}}$) detector arrays subject to photon noise unless the spectral bandwidth viewed by each detector is restricted. The current accepted method is to post-disperse the signal from the FTS using a reflection diffraction grating. In this paper, we present the design and performance verification of a diffraction grating spectrometer operated at cryogenic temperatures ($\sim$4 K) and used to disperse the output from a high-resolution (0.016 cm^{-1}) Martin-Puplett polarizing FTS [1] at room temperature forming a hybrid instrument concept: the **P**ost-**D**ispersed **P**olarizing **FTS** (PDPFTS).

Grating Concept

The diffraction grating spectrometer is based on the Czerny-Turner monochromator configuration [2]:

$$m\lambda = 2d\sin(\theta)\cos\phi. \quad (1)$$

m: order of diffraction, d: slit spacing, λ: wavelength, θ: incident angle, 2ϕ: deviation angle. The theoretical resolving power, R, was calculated under the assumption that it was slit width limited [3]:

$$R = \frac{m\lambda r'}{\max(w'', w')d\cos(\theta - \phi)}, \quad (2)$$

where r' is the focal length of the exit optic. The entrance slit width, w, was chosen so that the image width, w'', matched the exit slit, w', and achieved $R \sim$100 at 392.5 µm.

Design

Table 1: Design specifications for the grating spectrometer designed to operate in the 285 - 500 µm region.

Parameter	Value
Grating dimensions, (width x length)	105 mm x 50 mm
Slit spacing, d	312 µm
Deviation angle, 2ϕ	15°
Entrance slit width, w	5.0 mm
Exit slit width, w''	4.0 mm
Blaze angle, θ_B	39.4°

Key components of the grating spectrometer as shown in figure 1:

- **Monolithic grating enclosure**
- **50 mm entrance aperture/thermal filter**
- **Diffraction grating**
- **Rear-mounted flat mirror**
- **Baffle**
- **Exit Slit**
- **0.3 K Bolometer detector**
- **Enclosure shields**

The performance of the grating was studied using a calibrated blackbody source producing continuum radiation and a monochromatic, tunable terahertz photomixer. Light from the source(s) was modulated by the room-temperature FTS and passed into the cryostat where it was collimated and fed into the grating spectrometer as shown in figure 2. The two metrics of performance measured in this paper are the grating **efficiency** and **spectral resolving power**.

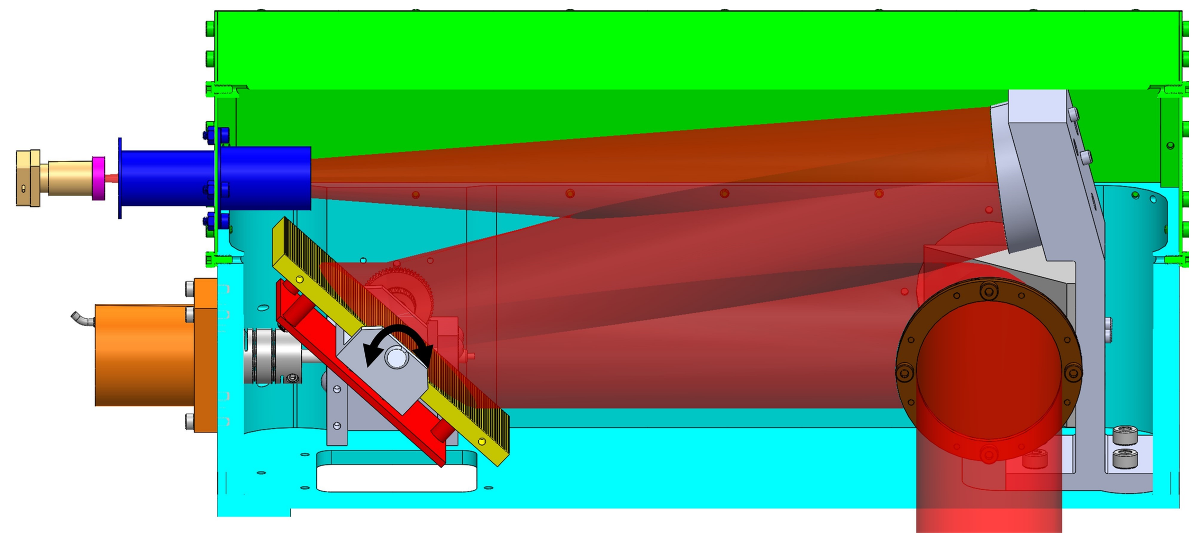

Figure 1: CAD rendering showing a cut-away view of the diffraction grating spectrometer. The grating rotates about the axis indicated by the arrow.

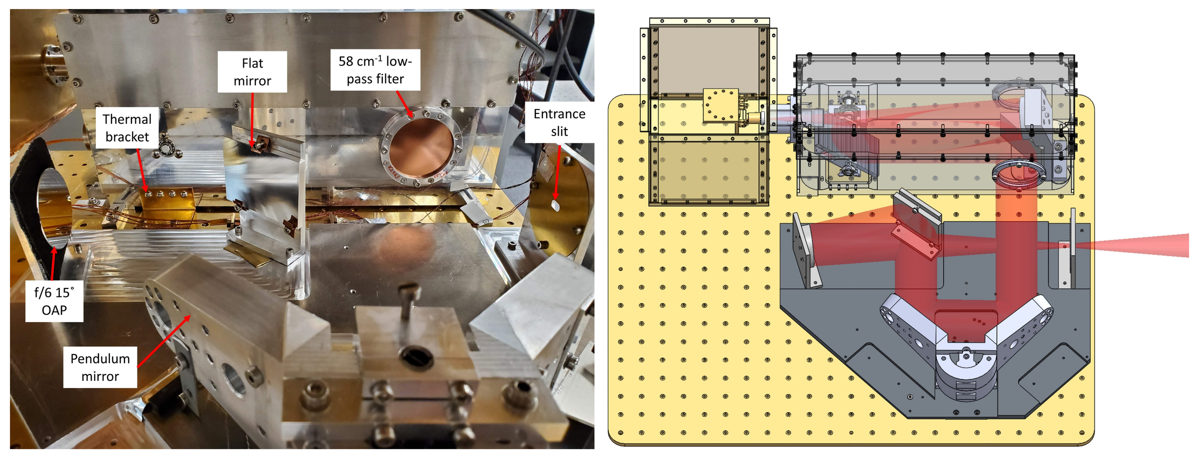

Figure 2: Grating spectrometer and auxilliary optical components [4] shown mounted in the 4 K volume of a test facility cryostat [5].

Results and Conclusions

Polarization Efficiency

Figure 3 presents measurements of the PDPFTS viewing a blackbody source with the FTS output polarized perpendicular (s-plane) and parallel (p-plane) to the grooves of the grating. Each coloured figure represents a spectral response function (SRF) obtained by scanning the polarizing FTS at each angular (wavelength) position of the grating. The black curve is the FTS spectrum obtained when the mirror was in the optical path. The features in the spectrum are signatures of molecular absorption within the 8.6 cm atmospheric path, and channel fringes caused by chamber windows.

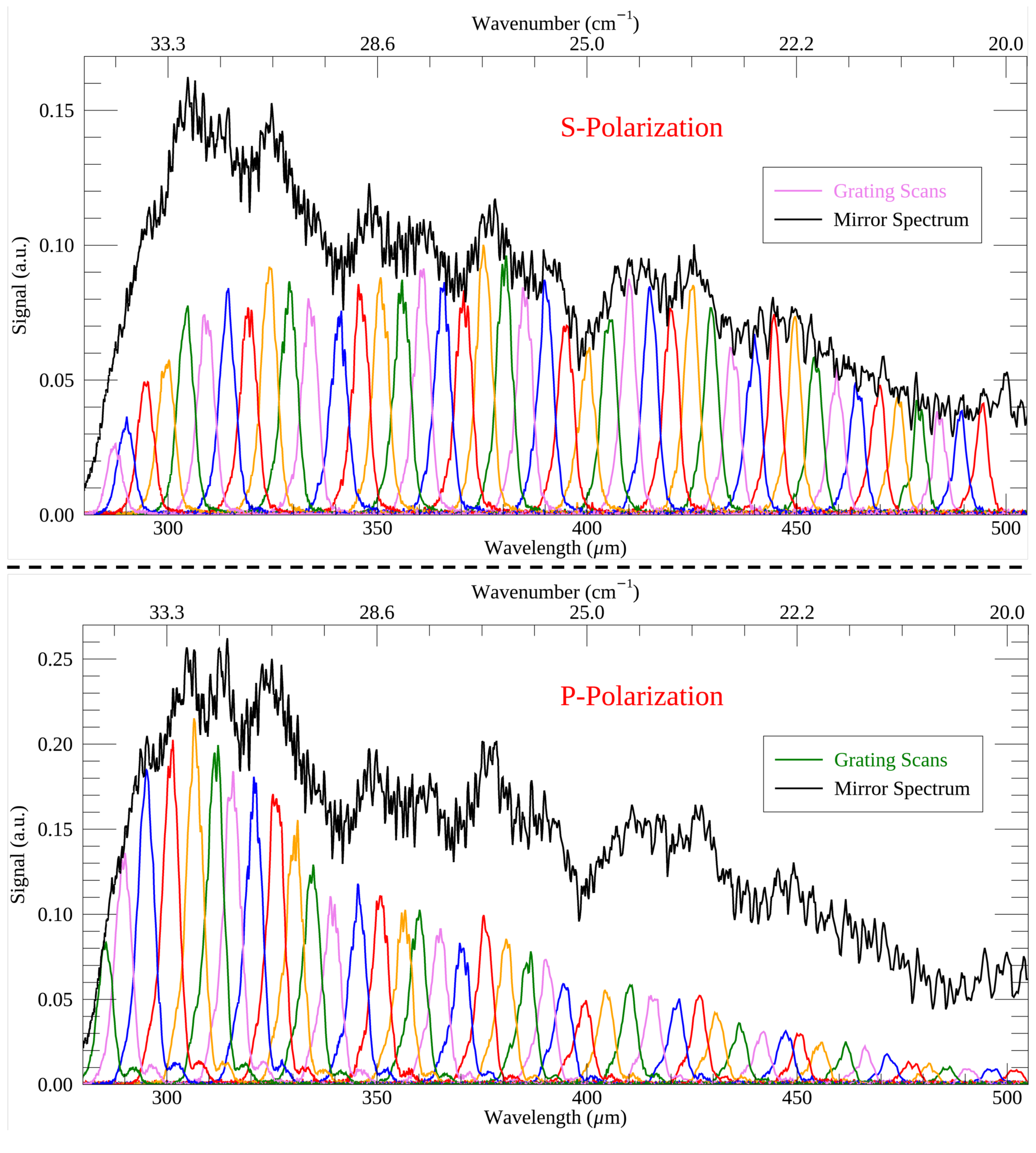

Figure 3: Measurements taken with the PDPFTS and a blackbody source.

The efficiency of the diffraction grating is shown in figure 4 for both polarization states. The theoretical model was determined numerically using the methods of Chandezon *et al.* [6].

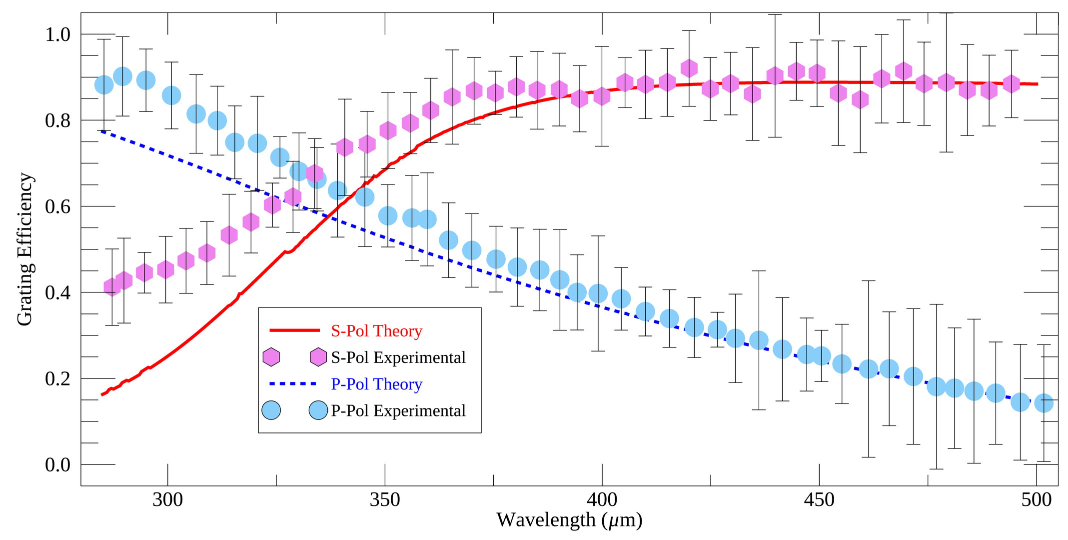

Figure 4: Diffraction efficiency measurements of s-polarized (pink hexagons) and p-polarized (blue circles) light compared to a theoretical model [6]. The deviations from the model at short wavelengths are likely due to machining imperfections not accounted for.

Resolving Power

Figure 5 shows three grating SRFs measured with the blackbody (top) and with the photomixer (bottom).

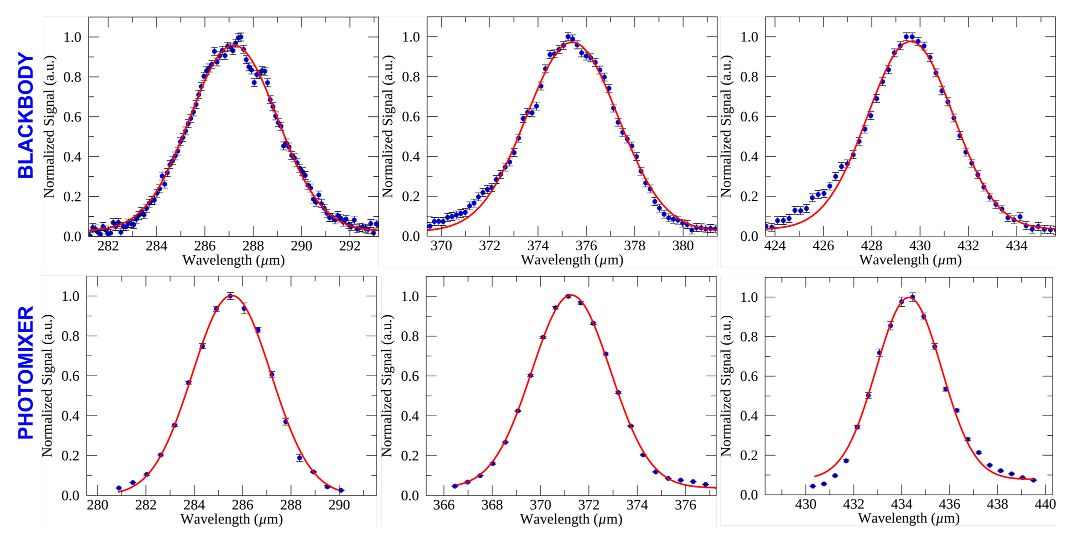

Figure 5: Measured signal (blue) and the best fit Gaussian profile (red).

Measurements were taken across the band and fit with a Gaussian equation to extract the center wavelength, λ_c, and full-width-half-maximum, $\Delta\lambda$, which were used to determine experimental R:

$$R = \frac{\lambda_c}{\Delta\lambda}. \quad (3)$$

The measured (3) and theoretical (2) resolving powers are compared in figure 6 for s-polarized light.

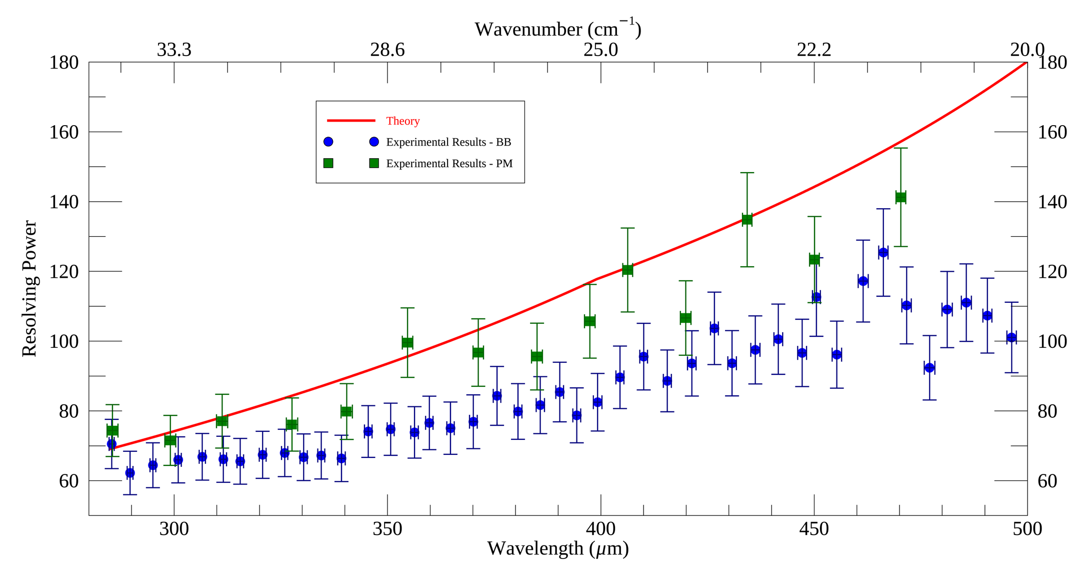

Figure 6: Experimental resolving power of the grating with the blackbody, BB, source (blue circles) compared with the photomixer, PM, (green squares). Both data follow the overall trend in R, however, we believe the lower R from the BB data is caused by smile distortion from the parabolic mirrors. The smile effect is more significant with the BB due to the size of the emitting element (3 mm vs 100 µm for the PM).

Conclusions

Future work will incorporate a cryogenic source module and cryogenic FTS module (FTSM) which will be operated in a large facility cryostat. A cryogenic photomixer has already been procured along with a cryogenic blackbody source which will allow the complete validation of the grating spectrometer at 4 K.

References

[1] Blue Sky Spectroscopy Inc. http://blueskyspectroscopy.com

[2] Czerny, M. and Turner, A. F., “ *U*ber den Astigmatismus bei Spiegelspektrometern”, Zeitschrift fur Physik, vol. 61, no. 11–12, pp. 792–797, (1930).

[3] Palmer, C. A., and Loewen, E. G., “Diffraction Grating Handbook,” Rochester, N.Y: Thermo RGL, (2002).

[4] Veenendaal, I., *et al.*, "An angle-scanned cryogenic Fabry–Pérot interferometer for far-infrared astronomy", Review of Scientific Instruments 91, 083108 (2020).

[5] Veenendaal, I., *et al.*, "Performance of a cryogenic test facility for 4 K interferometer delay line investigations," Proc. SPIE 9904, Space Telescopes and Instrumentation 2016: Optical, Infrared, and Millimeter Wave, 99045E (2016).

[6] Chandezon, J., Raoult, G., and Maystre, D., “A new theoretical method for diffraction gratings and its numerical application”, Journal of Optics, vol. 11, no. 4, pp. 235–241 (1980).

Acknowledgments

This research was funded in part by Alberta Innovates, Blue Sky Spectroscopy, CFI, CMC, CSA, NSERC, NTCO, and ULethbridge.